The Possible Role of Symmetric Instability in the Formation of Precipitation Bands

MARC A. SELTZER,* R. E. PASSARELLI AND K. A. EMANUEL

Center for Meteorology and Physical Oceanography, Massachusetts Institute of Technology, Cambridge, MA 02139

(Manuscript received 4 September 1984, in final form 7 May 1985)

ABSTRACT

Fifteen cases of banded and nonbanded precipitation not associated with surface frontal regions are presented. Results from the linear perturbation and parcel theories of symmetric instability are compared to the observed properties of these bands. Symmetric instability can explain many of the features of the bands considered in this study: all of the bands are aligned parallel to the thermal wind; strong shear and near-neutral static stabilities are observed when bands occur; multiple bands have a wavelength that is related to the depth of the unstable region and the slope of moist isentropic surfaces. However, the linear theory of symmetric instability assumes a basic state of unidirectional flow and thermal wind balance, while the observations indicate that in some cases these conditions are not met. This study supports the hypothesis that symmetric instability may be responsible for precipitation bands, but the comparison between theory and observations is hampered by the inability of the present theory to account for ageostrophic shear and curved flow, and our inability to assess geostrophy via sparse soundings.

1. Introduction

"It is now well established that the regions of heaviest precipitation in extratropical cyclones are often organized on the mesoscale in the form of rainbands" (Parsons and Hobbs, 1983). Some of these bands are directly associated with frontal circulations. Others occur far from any regions of frontal forcing. While much is known about mesoscale bands caused by frontogenesis, it is clear that not all bands, particularly multiple bands, are caused by frontogenesis. In this paper, the possible role of symmetric instability in the formation of precipitation bands is examined.

The data set used in this study was obtained during the M.I.T. NEWS (New England Winter Storms) Project. During three winters, 1981/82–1983/84, observations were taken from 20 storms with Doppler radar, aircraft, and standard National Weather Service data. In many of these storms intense precipitation bands occurred that were clearly not frontal in nature. These bands were usually embedded in regions of very strong shear and near-neutral static stability.

This paper will attempt to answer three questions:

1) How do the observed atmospheric conditions during these storms compare to those assumed in theoretical models of symmetric instability?

2) Do the observed precipitation bands exhibit those features predicted by the theory of symmetric instability?

3) Using simple linear and parcel theory, how well can one predict the occurrence of these bands, and in so doing, say something about their strength, structure and orientation?

Symmetric instability is a form of convective instability that can occur in baroclinic flows. It arises from an unstable balance of pressure gradient, Coriolis and buoyancy forces. Early investigations of the instability mechanism by Solberg (1936), Eliassen (1962), Stone (1966) and Ooyama (1966) focused on the linear stability of simple inviscid, balanced baroclinic flows in the context of an f-plane or a circular vortex. The basic findings of these studies indicated that symmetric instability sets in when the absolute vorticity vector of the flow has a shallower slope than that of isentropic surfaces. For zonal flow on an f-plane, a sufficient condition for instability is

$$\frac{\eta}{f}\mathrm{Ri} < 1, \tag{1.1}$$

where Ri is the Richardson number (N^2/U_z^2, where N is the buoyancy frequency and U_z is the vertical shear of the zonal wind), η is the vertical component of absolute vorticity, and f is the Coriolis parameter. The instability sets in as stationary roll circulations which do not vary in the direction of the thermal wind (thus, in a circular vortex, they are "symmetric") and which tend to line up with isentropic surfaces. The most unstable modes in an inviscid fluid were shown by Stone (1966) to have zero wavelength in the cross-shear direction. Emanuel (1979), however, showed that the addition of a small amount of viscosity leads to a preferred mesoscale wavelength proportional to the depth of the unstable layer divided by the slope of isentropic surfaces. Symmetric instability is thus a true mesoscale

* Present affiliation: Centre National de Recherches Meteorologiques, Toulouse Cedex, France.

instability characterized by order one Rossby number. Concurrently, Bennetts and Hoskins (1979) showed that the characteristics of the instability in a saturated, cloudy atmosphere could easily be assessed by comparing the orientation of the mean absolute vorticity vector to the slope of surfaces of constant equivalent potential temperature (θ_e), rather than potential temperature. The criterion for instability is identical to (1.1) but with the definition of the buoyancy frequency in Ri replaced by

$$N_m^2 = \frac{\Gamma_m}{\Gamma_d} \frac{g}{\bar{\theta}_e} \frac{\partial \theta_e}{\partial z},$$

where Γ_d and Γ_m are the dry and moist adiabatic lapse rates, respectively (Durran and Klemp, 1982). The effect of latent heat release is clearly destabilizing.

Certain nonlinear aspects of moist conditional symmetric instability were examined by Emanuel (1983a,b) who showed that the convection is sufficiently local to treat using parcel theory. He developed a straightforward analogue to the classical assessment of conditional instability using tephigrams, where the temperature of a lifted parcel is compared to its environment. In the generalized method, the parcel, rather than being lifted vertically, is lifted slantwise along a surface of constant absolute momentum M, where

$$M \equiv v + fx;$$

v is the component of geostrophic wind in the direction of the thermal wind and x is the coordinate across the thermal wind. The adiabatic temperature of the parcel is then compared to that of its environment in the usual way.

This parcel technique can be applied to a single sounding. Emanuel (1983b) has shown that for v varying linearly in x, the stability of a slantwise displaced parcel can be evaluated approximately by adding the value

$$\frac{1}{2} \frac{T_{vp}}{g} \frac{f}{\eta} \frac{\partial}{\partial z} [(v - v_p)^2]$$

to the reversibly lifted parcel temperature calculated in the usual way on a thermodynamic diagram. The virtual temperature of the parcel is expressed by T_{vp}. The lifting of a parcel in this manner is equivalent to the local slantwise displacement of a parcel that conserves both its M and θ values. Parcels can then be lifted from different heights in a manner analogous to that of assessing ordinary (buoyant) convection. The level and orientation of the most unstable parcels for finite lifting can be determined by varying both the initial height and orientation of the parcel (or tube).

Further support of this explanation of banded precipitation must come from a comparison between the observations of atmospheric conditions in the vicinity of banded precipitation and the linear theory. For example, there are several observational checks that can be made:

1) The atmospheric conditions should be approximately two-dimensional with most of the variations in thermodynamic and kinematic properties occurring in the cross-band direction and in the vertical.

2) There should be a region in the atmosphere where the local Richardson number instability criterion for saturated conditions [e.g., Eq. (1.1)] is met.

3) The bands should be aligned along the thermal wind and should be strongest in the region of instability.

4) If the bands are observed to be moving in the cross-band direction, they should be moving approximately with the mean flow in this direction. Note that the results of linear theory imply that the circulation pattern does not propagate relative to the basic-state flow in x.

5) Spacing between bands should be related to the depth of the unstable layer and the slope of moist isentropic surfaces.

6) The circulation pattern near the bands should include a region of ascending motion sloping nearly along moist isentropic surfaces.

2. Observations

The measurements of thermodynamics and kinematic properties for 15 cases were all taken from sounding data. Standard National Weather Service (NWS) balloon soundings from Chatham, Massachusetts; Portland, Maine and Albany, New York, launched at nominal times as well as special launch times were used. Rawinsondes were also launched from M.I.T. In addition, aircraft measurements made by the NOAA P-3 were taken in a sounding mode at locations chosen to best supplement the other soundings. Data from mandatory and significant levels of the NWS soundings were used. All sounding data were interpolated to a 250-m vertical grid.

The cases presented in this study were chosen to meet three requirements:

1) The low pressure center, as determined from surface analyses, was not within 500 km of the region of analysis. This requirement excluded regions that had a generally more complicated mesoscale structure involving frontal zones and strongly curved flow.

2) Precipitation was observed on the M.I.T. radar.

3) Surface fronts were not present in the region.

Table 1 lists the fifteen cases that will be considered in this study.

A measure of bandedness of the precipitation was determined for each case. This was done subjectively by four scientists (other than the authors and all experienced in observing bands) using radar reflectivity patterns such as that shown in Fig. 1. The criteria used to define bandedness were:

1) The elongation of the reflectivity distribution in the horizontal.

TABLE 1. Measurements of thermodynamic and kinematic properties from sounding data for fifteen cases.

Case mon/day/yr	Bandedness	B.O.	LMWS	FFS	DDS	N_d^2	N_m^2	850–500 mb FFS
12/05/81	3	45	4.75	13.5	37	1.4	0.7	8.0
12/06/81	3	0	2.75	13.3	5	1.6	0.8	8.3
12/16/81	3	45	1.75	18.6	39	2.0	0.7	3.0
12/11/82	1	70	4.00	11.2	55	6.9	4.0	5.2
12/12/82	2	50	3.75	17.1	51	2.3	1.0	14.6
12/20/82	2	0	2.00	14.5	−2	0.7	−2.7	6.7
01/11/83	3	0	3.00	19.4	14	2.5	1.4	4.2
01/24/83	0	—	4.25	8.2	129	1.3	0.2	5.0
02/03/83	0	—	3.25	7.9	90	2.4	1.5	3.3
02/12/83	3	80	5.50	13.4	66	1.8	1.1	9.4
11/28/83	3	135	2.75	21.2	117	3.0	2.5	4.9
12/03/83	1	90	5.75	11.5	115	0.8	0.3	6.6
12/04/83	0	—	5.25	22.4	63	2.2	1.2	5.7
12/06/83	0	—	2.00	9.6	120	3.8	−0.2	5.8
01/11/84	2	45	3.75	19.5	34	3.4	2.5	8.6

LMWS: level of maximum wind shear magnitude (km).
B.O.: band orientation (deg).
FFS: wind shear magnitude (m s^{-1} km^{-1}).
DDS: wind shear direction (deg).
N_d^2: buoyancy frequency (dry) (10^{-4} sec^{-2}).
N_m^2: buoyancy frequency (moist) (10^{-4} sec^{-2}).
Note: FFS, DDS, N_d^2, and N_m^2 computed at LMWS.

2) The strength of the reflectivity factor anomaly.
3) The band's temporal and spatial coherence.

A four-point scale was used, with 0 signifying nonbanded and 3 denoting strong bandedness.

a. The synoptic situation for a representative case

The cases classified as banded have some common synoptic-scale features. These features can be summarized by looking at a representative case which is described in greater detail in a separate paper (Passarelli *et al.*, 1986). Figure 2 shows the surface analysis for 0000 GMT 6 December 1981. The low-pressure center is well to the east of Boston and any obvious surface fronts are far from the New England area. Figure 3 shows the 500 mb geopotential height and temperature field for the same time. Note the strong horizontal temperature gradients corresponding to large geostrophic wind shears in the New England area.

The corresponding radar reflectivity pattern was shown previously in Fig. 1. This constant altitude presentation represents the average reflectivity in a layer from 2.5 to 4.0 km altitude. The dominant feature is a large band of very heavy precipitation oriented north–south. This particular band persisted for almost 14 hours in the New England area and produced snowfall rates of more than 5 cm h^{-1}. A comparison of Fig. 3 with Fig. 1 shows that the band is embedded within the region of very strong shear.

Analyses of potential temperature, equivalent potential temperature, and winds from a sounding at Portland, Maine (60 km from the band) are shown in Fig. 4. Again the region of strong shear is noted, as is a deep layer of positive static stability that includes the layer of banded precipitation. There is no obvious frontal zone and there are no large regions of neutral or negative stability. Most of the atmosphere is gravitationally stable. These observations would seem to rule out the occurrence of deep moist convection.

While many of the band cases discussed here are not as striking as the one just described, most of them exhibit similar synoptic scale features. The presence of strong band-parallel shear in all of the band cases makes symmetric instability a prime candidate for the mechanism responsible for the banded precipitation.

b. Mesoscale features of the cases studied

In this section, the atmospheric conditions that existed in each case are presented. The cases are compared and the common features are deduced.

As implied in the previous section, banded precipitation is often embedded in regions of strong shear. Table 1 lists, for each case, the shear direction, the shear magnitude, and the buoyancy frequency for dry and moist adiabatic ascent. All of these quantities are computed at the level of maximum wind shear. Also shown are the magnitude of the 850–500 mb wind shear, the estimated bandedness, and the band orientation. The data used to make these calculations come from the sounding that was taken closest to the band.

On comparing the cases, a strong correlation between the bandedness and the maximum wind shear becomes apparent. The nine cases classified with a level 2 or level 3 bandedness have a maximum wind shear magnitude between 13 and 20 m s^{-1} km^{-1}. The remaining

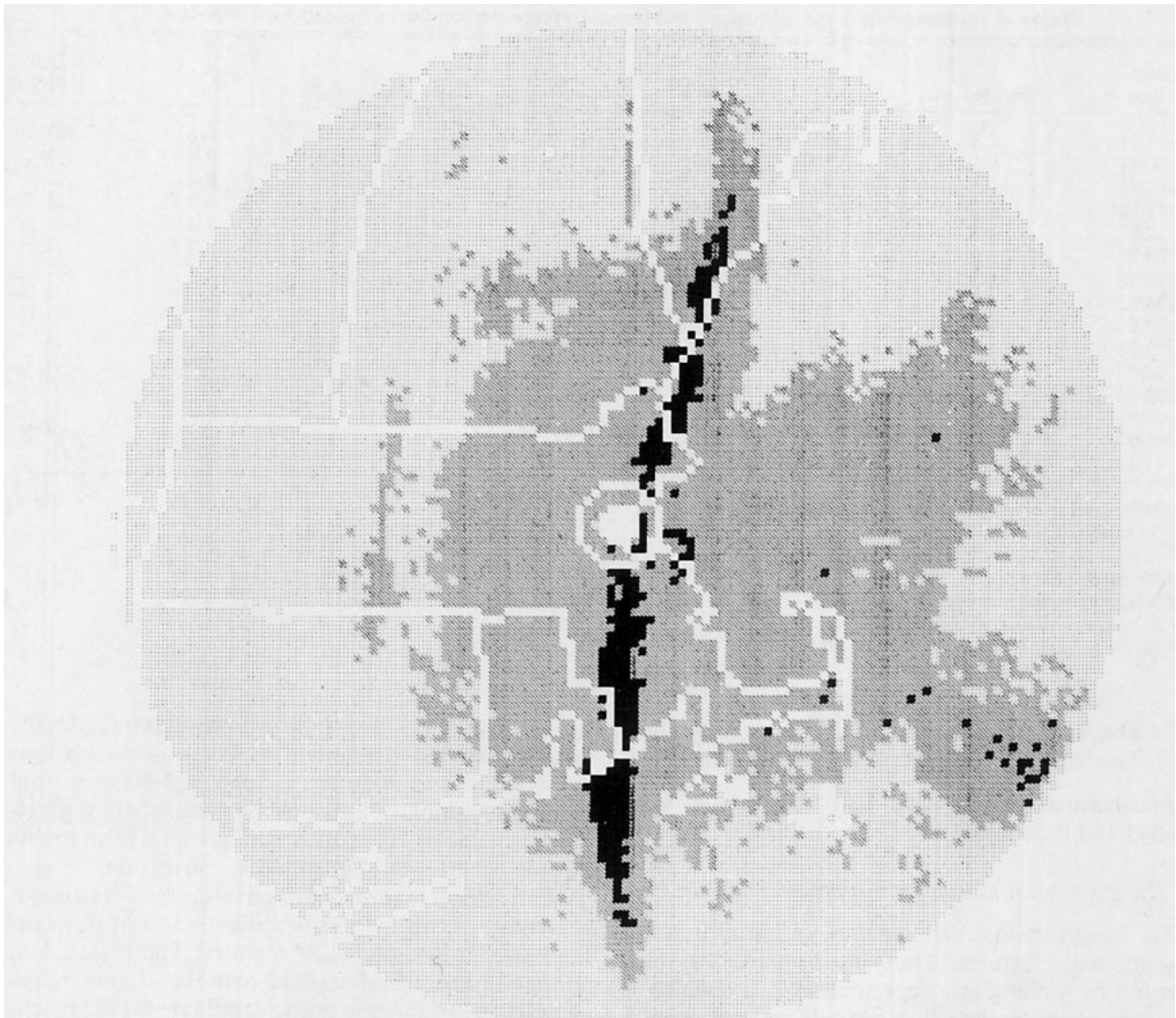

FIG. 1. Constant-altitude planned position indicator showing the average reflectivity factor in a layer from 2.5 to 4.0 km altitude for 0000 GMT 6 December 1981. Two contour levels of reflectivity factor are shown: 15 and 25 dbZ.

cases, classified as nonbanded or weakly banded, with the exception of 4 December 1983, have a maximum wind shear magnitude between 7 and 12 m s^{-1} km^{-1}. A much weaker correlation is evident when the level of bandedness is compared with the magnitude of the 850–500 mb wind shear.

Figure 5 is a scatter diagram for all nonzero band cases of the band orientation versus the 1000–500 mb geostrophic shear direction and the shear direction at the level of maximum wind shear. The latter direction is averaged over a 1 km layer. The errors in measuring the geostrophic shear direction and the mean shear direction are approximately ±10 and ±5 deg, respectively. The error in measuring the band orientation is about ±10 deg. While both measures of the shear direction are close to the band orientation, the geostrophic shear direction is in slightly better agreement. The rms scatter is 9.2 deg for the geostrophic shear direction versus 13.4 deg for the shear direction at the level of maximum shear.

Vertical profiles of the static stability were also analyzed for each case. It was found that all of the cases were stable for dry adiabatic ascent above the boundary layer. In the region of maximum wind shear, three of the band cases show an atmosphere that is neutral or potentially unstable for moist adiabatic ascent. There are, however, other regions of the atmosphere in many of the cases that show indications of potential instability ($\partial\theta_e/\partial z < 0$). A negative moist static stability is a sufficient condition for convective overturning only if the atmosphere is saturated.

For the cases considered in this study, the regions of potential instability that were judged saturated are only weakly unstable and can be considered, within the error of measurement, to be neutral. Regions that were assessed as having substantial potential instability

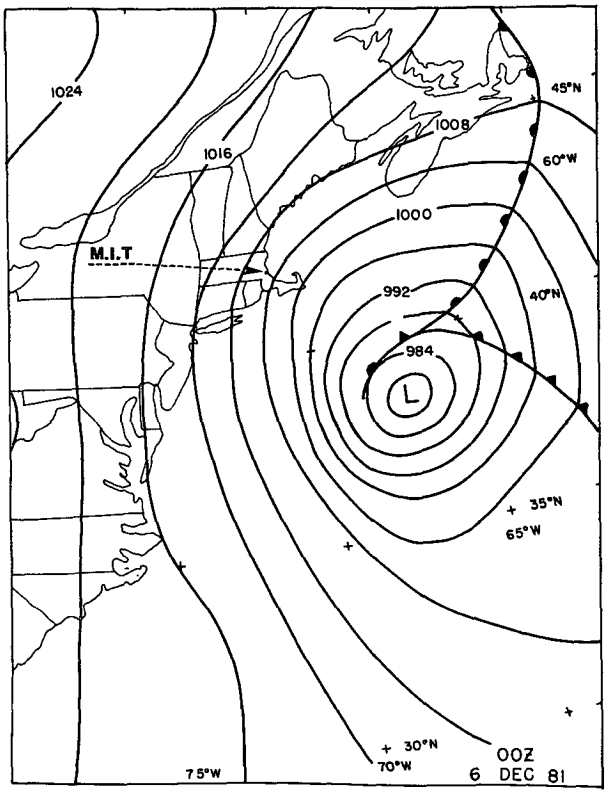

FIG. 2. Surface analysis for 0000 GMT 6 December 1981, adapted from National Meteorological Center (NMC) analysis.

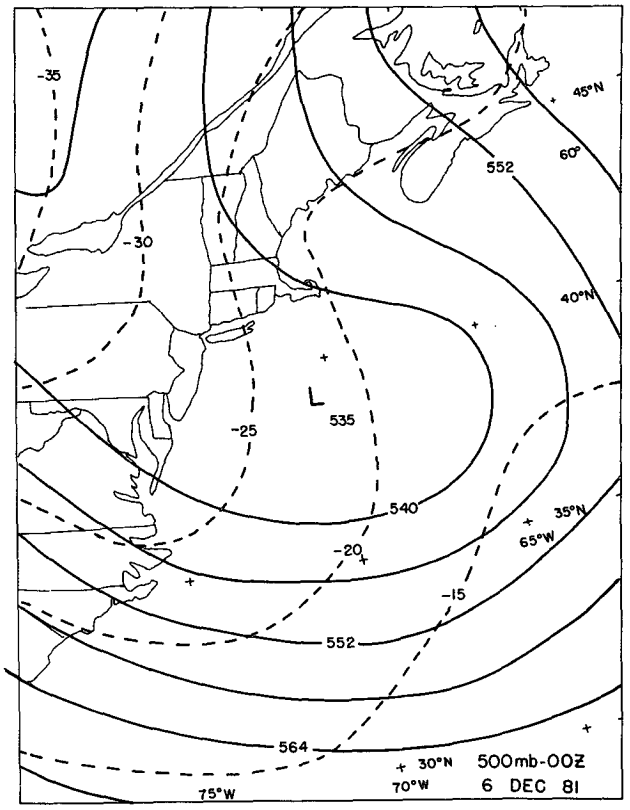

FIG. 3. 500 mb geopotential height (dam) and temperature (°C) analyses for 0000 GMT 6 December 1981, adapted from NMC analyses.

are in all cases associated with relative humidity gradients in an unsaturated atmosphere. In this instance, the potential instability may never be released.

Some evidence has already been given to justify the assumption that the bands are two-dimensional in nature. The bands are observed to be aligned close to the geostrophic shear vector which, in a geostrophically balanced atmosphere, is the direction perpendicular to the average temperature gradient. The band's thermodynamic properties can therefore be approximated as having most of their variations in the cross-band direction. In addition, Doppler radar and synoptic scale wind analyses provide evidence that most of the flow is in the band-parallel direction with variations in this flow occurring predominantly in the cross-band direction.

3. Comparisons between theory and observations

a. The assessments of symmetric instability

Stability analyses based on a single sounding were done for all cases. Richardson number analyses and the single-sounding parcel method analyses were used for this purpose. These analyses require the knowledge of the geostrophic absolute vorticity, $\eta = f + \partial v/\partial x$ as a function of height. The absolute vorticity was estimated from the Low-order Fine Mesh model (LFM)

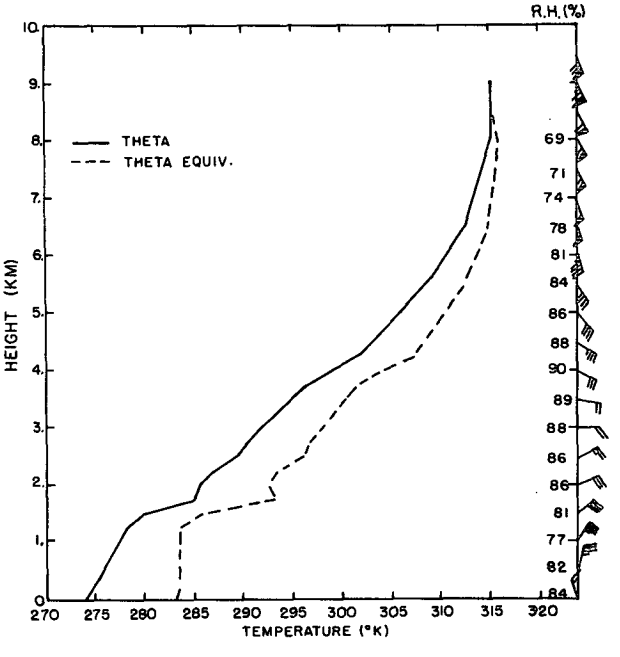

FIG. 4. Analyses of potential temperature (K), equivalent potential temperature (K), and winds from Portland, Me, at 0000 GMT 6 December 1981. Relative humidity values are indicated on the right.

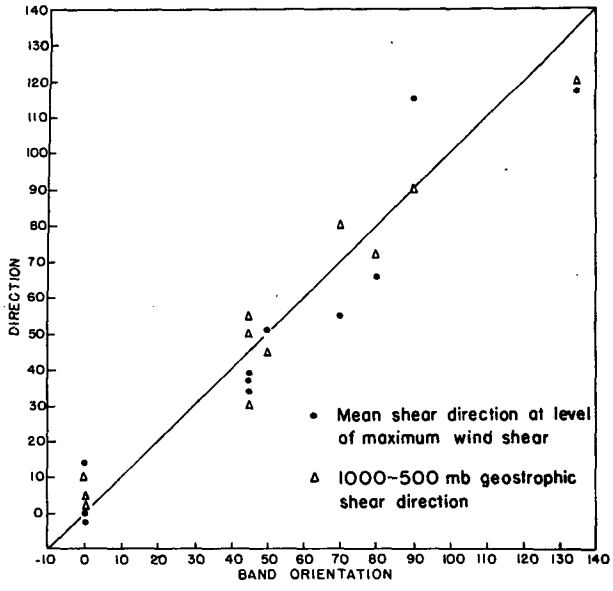

FIG. 5. Scatter diagram of the band orientation (deg) versus the 1000–500 mb geostrophic shear direction (deg) and the shear direction at the level of maximum wind shear.

500 mb vorticity fields for all cases. It was found that neglecting $\partial v/\partial x$ in the Richardson number and parcel theory analyses would lead to an error of only about ten percent. For this reason, the relative vorticity is neglected in the single-sounding stability analyses.

To demonstrate the assessment techniques which were applied, the sounding taken from Chatham, Massachusetts at 1200 GMT on 5 December 1981 is examined. At this time, a snow band (judged level 3) was observed in the vicinity of Chatham. As the band moved over Chatham approximately three hours later, the band orientation was 045 deg.

Figures 6a–d show vertical profiles of Ri^{-1}, θ, θ_e, and the magnitude of the component of wind shear parallel to the band. The Ri is calculated from the observed band-parallel wind shear, which is considered to represent the geostrophic basic state, and dry adiabatic ascent is assumed. Note that the layer between 4.0 and 6.0 km is nominally symmetrically unstable. The potential temperature and equivalent potential temperature profiles, on the other hand, show that the atmosphere is stable for both dry and moist adiabatic ascent. The profile of the shear magnitude indicates that the Richardson numbers less than one, observed between 4.0 and 6.0 km, result from the very strong shear in this layer.

The parcel method evaluation for this case is illustrated in Fig. 7. Plotted is the modified parcel temperature for the slantwise adiabatic ascent of an air parcel originating at 4.0 km height. The orientation of the parcel is assumed to be along the band-parallel direction (045°/225°). (Recall that a parcel refers to an infinitely long tube oriented along the direction of the band.) Also shown are the environmental and dewpoint temperatures, and the 283 K moist adiabat that passes through the parcel's starting position.

Conventional gravitational instability is evaluated by lifting the parcel vertically along its appropriate moist or dry adiabat and comparing the parcel temperature to the environment. Symmetric instability is evaluated by lifting the parcel along an estimate of a

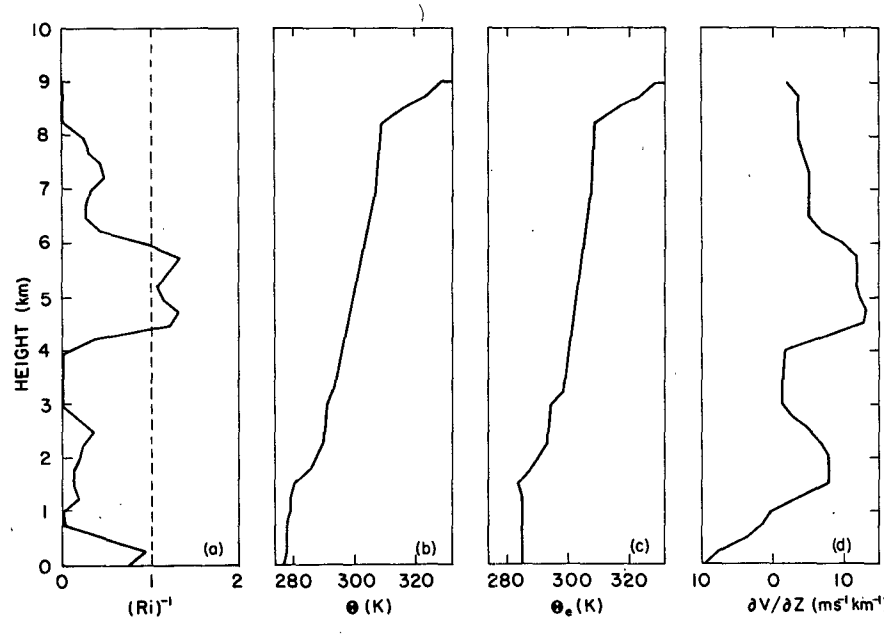

FIG. 6. Plots of (a) inverse Richardson number, (b) potential temperature (K), (c) equivalent potential temperature (K), and (d) the magnitude of the band-parallel wind shear (m s^{-1} km^{-1}) as functions of height (km).

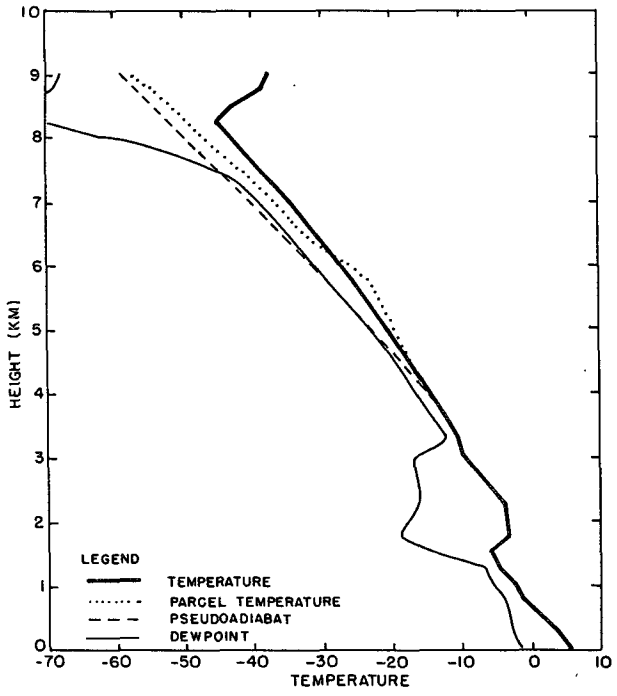

FIG. 7. Plots of the modified parcel temperature (°C) for the slantwise ascent of an air parcel originating at 4.0 km height, the environment and dewpoint temperature (°C), and the 283 K moist adiabat. The orientation of the parcel is assumed to be along the band-parallel direction (045°/225°).

constant M surface (labeled parcel temperature in the figure) and making the same temperature comparison. This analysis shows that while parcels originating near 4.0 km are completely stable to vertical displacements, they are unstable to slantwise displacements up to a height of 6.25 km.

Figure 8 shows contours of the maximum temperature difference between a parcel and its environment during lifting to 9.5 km for different starting heights and parcel (or tube) orientations. There is a well-defined maximum of 2.5°C at a height of 4.0 km for an orientation angle of 030°/210°. The analysis further indicates that all parcels originating between 3.25 and 5.5 km with an orientation angle between 30 and 60 deg are unstable to slantwise lifting. The depth and height of the layer of maximum symmetric instability agree with the Richardson number analysis.

b. Results of single-sounding analyses

The parcel method can be used to predict the strength and orientation of banded precipitation. In the previous example, parcel theory predicts that the band will be oriented at 030°/210°. The strength of the band should be related to the predicted parcel temperature surplus. The actual correlation between this temperature surplus and bandedness will be examined after assessing by more conventional means the symmetric stability for all band cases.

Table 2 lists for each case the minimum value of the Richardson number for dry and moist adiabatic ascent and descent, and the level of the minimum dry Richardson number. When the environment in the region of minimum Richardson number is not saturated, only the Richardson number for dry ascent is presented. The magnitude of the band-parallel wind shear is used to compute the Richardson number for the banded cases. The magnitude of the wind shear in the direction of the 1000–500 mb geostrophic shear is used to compute the Richardson number for the nonbanded cases.

For comparison to Table 1, many of the parameters listed there are included in Table 2. The parameters listed are computed at the level of minimum Richardson number calculated for dry ascent. This level will subsequently be referred to as the level of maximum instability (LMI). In all of the cases, the level of minimum Richardson number is the same for both dry and saturated conditions. The boundary layer up to 1.5 km is excluded from all calculations in an attempt to exclude regions where surface viscous forces are important. In these regions the inviscid theory may not be valid.

It is evident that in all but one of the band cases, the LMI is within 250 m of the level of maximum wind shear. This implies that the indications of symmetric instability result from the strong shear. Any change in static stability with altitude has only a small effect on the level of the critical Richardson number. The pos-

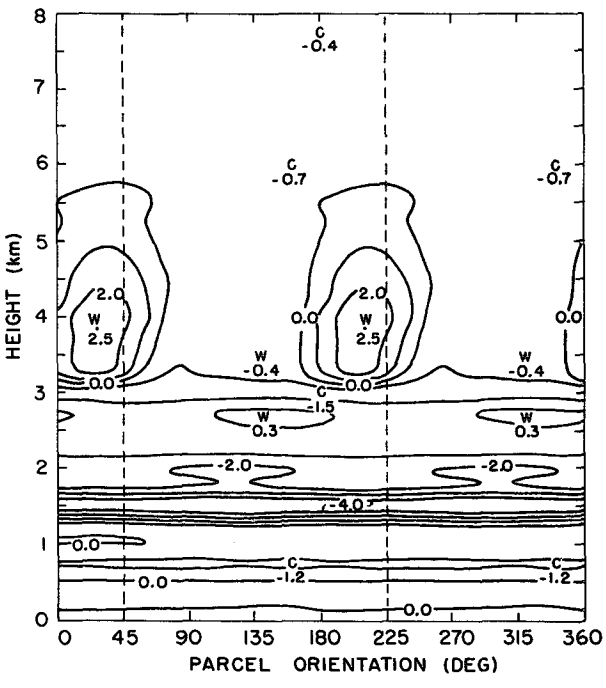

FIG. 8. Contours of the maximum temperature difference (°C) between a parcel and its environment during lifting to 9.5 km as a function of starting height (km) and parcel orientation (deg) at 1200 GMT 5 December 1981. Dashed line indicates the band orientation.

TABLE 2. The minimum value of the Richardson number for dry and moist adiabatic ascent and descent.

Case (mon/day/yr)	Bandedness	B.O.	LMWS	LMI	Ri dry	Ri moist
12/05/81	3	45	4.75	5.00	0.76	0.36
12/06/81	3	0	2.75	2.75	0.93	0.40
12/16/81	3	45	1.75	1.75	0.58	0.18
12/11/82	1	70	4.00	4.00	1.93	1.16
12/12/82	2	50	3.75	4.00	0.43	0.02
12/20/82	2	0	2.00	2.00	0.32	*
01/11/83	3	0	3.00	3.00	0.79	*
01/24/83	0		4.25	4.25	5.10	1.57
02/03/83	0		3.25	5.00	1.27	*
02/12/83	3	80	5.50	5.25	0.68	0.27
11/28/83	3	135	2.75	2.75	0.86	0.53
12/03/83	1	90	5.75	5.75	0.62	0.10
12/04/83	0		5.25	5.25	0.68	0.38
12/06/83	0		2.00	3.25	1.13	*
01/11/84	2	45	3.75	3.75	0.92	0.70

* Environment not saturated at LMI.
B.O.: band orientation (deg).
LMWS: level of maximum wind shear (km).
LMI: level of maximum instability (km).

itive correlation between bandedness and maximum shear magnitude that was observed in Section 2 is therefore essentially the same as the positive correlation between bandedness and minimum Richardson number that is evident in Table 2. In ten of the eleven band cases, the minimum Ri is less than the critical value (Ri = 1) needed for instability, while in three of the four no-band cases the minimum Ri is greater than one.

Table 3 summarizes the assessment of symmetric instability by the single sounding parcel method for all cases studied. The same analysis technique used with Fig. 10 is applied. Parcels are lifted slantwise from starting levels between 1.5 and 7 km to a height of 9.5

TABLE 3. Symmetric instability assessed by the single sounding parcel method for all cases studied.

Case (mon/day/yr)	Bandedness	B.O.	LMI	MTS	LMTS	P.O.	LUP
12/05/81	3	45	5.00	2.5	3.75	30	3.25–5.50
12/06/81	3	0	2.75	2.8	2.25	0	2.00–2.50
12/16/81	3	45	1.75	1.2	1.50	40	1.50–1.75
12/11/82	1	70	4.00	0.0	3.00	*	**
12/12/82	2	50	4.00	6.0	3.50	60	3.00–5.00
12/20/82	2	0	2.00	2.1	1.50	−10	1.50–2.00
01/11/83	3	0	3.00	3.2	1.75	20	1.50–2.50
01/24/83	0		4.25	0.2	7.00	140	7.00
02/03/83	0		5.00	1.1	5.50	130	5.50
02/12/83	3	80	5.25	4.7	3.50	45	2.50–5.25
11/28/83	3	135	2.75	6.4	2.25	120	1.75–3.75
12/03/83	1	90	5.75	0.8	5.00	110	4.50–6.00
12/04/83	0		5.25	1.7	4.75	*	4.50–6.50
12/06/83	0		3.25	−0.5	3.50	*	**
01/11/84	2	45	3.75	2.7	2.75	50	1.50–3.50

Bandedness: rated on a scale of 0–3; see text for criteria.
B.O.: band orientation (deg).
LMI: level of maximum instability (km).
MTS: maximumm parcel temperature surplus (°C).
LMTS: level of MTS (km).
P.O.: predicted orientation angle (deg).
LUP: layer in which unstable parcels originate (km).
* No preferred orientation.
** No unstable parcels.

km for all possible band orientations. From the resulting plots the following quantities are read and listed in Table 3: level and magnitude of maximum parcel-temperature surplus; prediction of band orientation; and layer in which unstable parcels originate. In eight of the 11 band cases, the LMI determined from Richardson number analyses is within the layer of unstable parcels. In two band cases the LMI is within 500 m of this layer. One band case has no layer of unstable parcels. On average the stronger band cases have a larger maximum parcel temperature surplus (MTS) and a deeper layer of instability.

A two-sample rank test (Mann and Whitney, 1947) was performed in order to differentiate the nonbanded and weakly banded events (judged level 0 and 1 bandedness) from the more strongly banded events (judged level 2 and 3 bandedness). At the 95% confidence level, it was found that the events judged level 2 and 3 bandedness have, stochastically, larger maximum band-parallel shear, a smaller minimum Richardson number, and a greater maximum parcel temperature surplus.

Figure 9 shows the actual band orientation, the predicted orientation and the 1000–500 mb geostrophic shear direction. The predicted orientation is calculated to the nearest 10 deg. In six of the 11 band cases, the predicted orientation angle is as close as or closer than the 1000–500 mb geostrophic shear direction is to the band orientation.

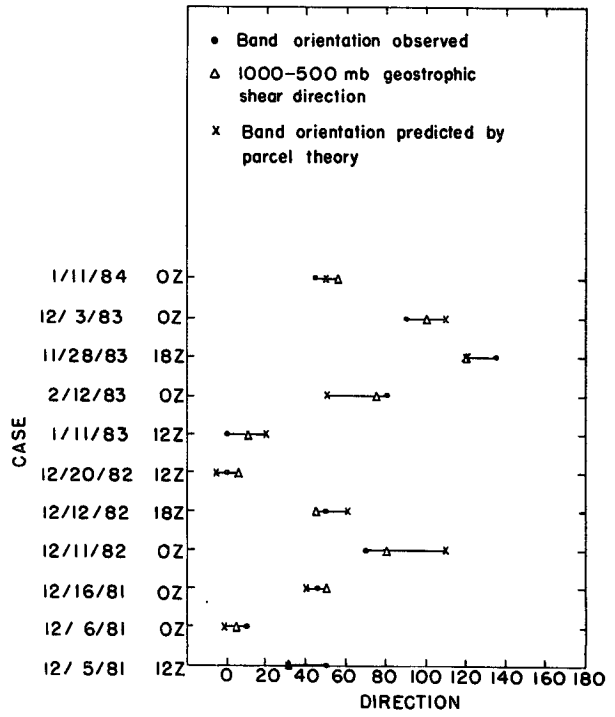

FIG. 9. Comparison of the actual band orientation, the predicted orientation, and the 1000–500 mb geostrophic shear direction for each band case.

TABLE 4. Predicted versus observed wavelengths for four cases.

Case (mon/day/yr)	Observed wavelength (km)	Predicted wavelength (km)
12/12/82	45	48
01/11/83	55	35
11/28/83	115	81
01/11/84	65	113

Other comparisons can be made with the linear theory. Recall that linear theory with viscosity predicts that the spacing between bands should be related to the depth of the unstable region and to the slope of the isentropes. An order of magnitude estimate for this predicted wavelength can be obtained from a simple scaling analysis. Let H be the depth of the unstable region. The slope α of the moist isentropes is given by

$$\alpha = -(\partial\theta_e/\partial x)/(\partial\theta_e/\partial z). \tag{3.1}$$

Thus the predicted wavelength L can be approximated by

$$L \sim \frac{H}{|\alpha|}. \tag{3.2}$$

If the thermal wind relation is used to express the horizontal temperature gradient in terms of the geostrophic wind shear, L can be written in finite difference form as

$$L \sim \frac{Hg}{f\bar{\theta}_e}\frac{\Gamma_m}{\Gamma_d}\frac{\Delta\theta_e}{\Delta V} \tag{3.3}$$

where $\Delta\theta_e$ and ΔV are evaluated across the level of maximum instability.

Multiple bands were observed in four of the band cases. The observed wavelength was measured from radar reflectivity maps. Table 4 shows that the wavelength predicted by Eq. (3.3) agrees well with the observed wavelength in three of the four cases.

The present linear theory also implies that the bands should not propagate relative to the mean flow in the unstable region. Figure 10a–e shows the observed speed of the band along with vertical profiles of the observed cross-band wind speed for the five bands judged to have level 3 bandedness. The level 3 band cases were chosen for this comparison because they were the easiest to follow in time. The region of maximum instability as assessed from the dry Richardson number condition is hatched and the layer of unstable parcels is denoted at the right-hand side of the figures. The cross-band wind profile is taken from the sounding nearest to the band, but not in the band, in order to minimize the influence of the band itself. However, it is likely that the wind soundings themselves are influenced by the perturbations, whose magnitude may be comparable

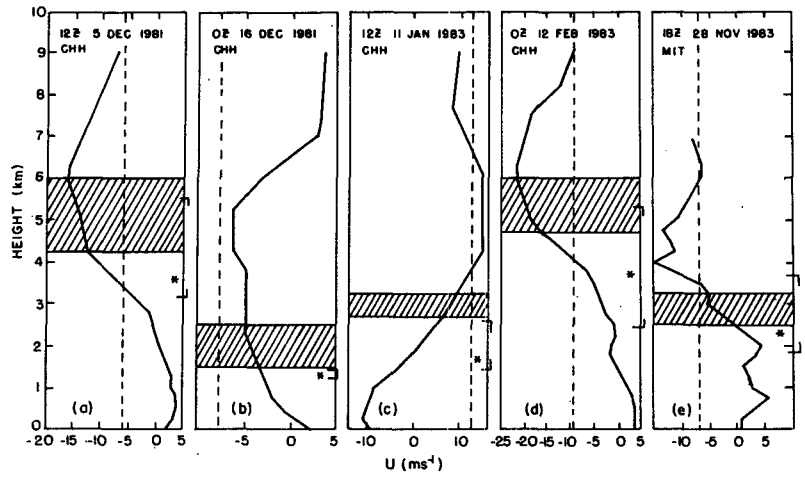

FIG. 10. The observed cross-band wind speed (m s^{-1}) as a function of height (km) for (a) 1200 GMT 5 December 1981, (b) 0000 GMT 16 December 1981, (c) 1200 GMT 11 January 1983, (d) 0000 GMT 12 February 1983, (e) 1800 GMT 28 November 1983. Region of instability as assessed from Richardson number analysis is hatched. The level of maximum temperature surplus is denoted by an asterisk, while the layer of unstable parcels is bracketed as shown.

to that of the mean flow (Emanuel, 1983a). Note that positive u is defined as toward the warm air.

The five bands studied are all moving at speeds corresponding to cross-band winds in the midtroposphere (between 3 and 5 km height). None of the bands is moving with the cross-band wind in the region of maximum instability, but three of the five bands are moving with winds in the origin layer of unstable parcels. In four of the five cases, the altitude where the two speeds match is within a kilometer of the unstable region.

It is also evident from the figures that there is substantial shear of the cross-band wind within the unstable layer. Shears of 2–5 m s^{-1} km^{-1} are observed in this layer. While such shear magnitudes are much less than the band-parallel shears in these regions (13–21 m s^{-1} km^{-1}), they are not negligible. It is quite likely that these cross-band winds are reflections of the presence of the band circulations themselves.

c. *The geostrophy of the observed wind shear*

In all of the previous assessments of the symmetric stability of the atmosphere it was assumed that the observed winds were representative of the geostrophically-balanced basic state. In particular, in the Richardson number analyses, it was assumed that the observed band-parallel wind shear is equal to the geostrophic shear.

It was shown in Fig. 7 that the band orientation tends to be close to the geostrophic shear direction. Even if these two directions differ by 15 deg, the magnitude of the band-parallel wind shear will differ by only 4 percent from the geostrophic wind shear as a result of choosing the wrong direction. Therefore an estimate of the cross-band temperature gradient can be used to calculate the magnitude of the geostrophic shear. For each band case, two soundings on opposite sides of the band are used to estimate the temperature gradient between the two stations. The sounding locations are projected normally onto a line perpendicular to the band orientation. The magnitude of the geostrophic wind shear is, from the thermal wind relation,

$$\frac{\partial V_g}{\partial z} \approx \frac{g}{f\bar{\theta}} \frac{\Delta\theta}{\Delta x},$$

where Δx is the distance between the two projected sounding locations and $\Delta\theta$ is the potential temperature difference evaluated at any given height. Note that this estimate of the temperature gradient is really a lower bound estimate of the maximum temperature gradient that could exist.

For five cases where the necessary soundings were available, vertical profiles of the estimated geostrophic shear and the band-parallel shear were plotted (not shown). The band-parallel shear is determined from the sounding nearest to the band. This is the same sounding that is used in the single sounding Richardson number analysis.

From comparison of the profiles it was found that in many regions of the atmosphere, the two shear magnitudes were markedly different. Table 5 lists the average band-parallel shear in the region of instability (i.e., where $Ri < 1$) and the estimated geostrophic shear in this region. The agreement is not good. In all five cases, the observed wind shear is supergeostrophic in the region of maximum instability. These discrepencies prompted a reassessment of the symmetric stability of

TABLE 5. Band-parallel versus geostrophic wind shears.

Case (mon/day/yr)	Average band-parallel wind shear (m s^{-1} km^{-1})	Average estimated geostrophic wind shear (m s^{-1} km^{-1})
12/05/81	12.5	6.5
12/11/82	9.0*	4.0*
12/20/82	12.4	6.8
01/11/83	11.3	8.7
01/11/84	12.2	5.4

* Value computed at level of maximum wind shear. All other values are computed in the region of maximum instability.

Note: There is no region of maximum instability for the case of 12/11/82.

the atmosphere substituting the geostrophic wind shear for the observed. The Richardson number condition of Eq. (1.1) was used for this reassessment. This can be written in terms of the horizontal temperature gradient as

$$\mathrm{Ri} = \left(\frac{f\bar{\theta}N}{g(\partial\theta/\partial x)}\right)^2 < 1,$$

or equivalently as

$$\frac{\partial\theta}{\partial x} > \frac{f\bar{\theta}}{g} N. \tag{3.4}$$

The quantity on the right-hand side of Eq. (3.4) is therefore the critical value of the temperature gradient for instability. If the observed temperature gradient is greater than this critical gradient, perturbations from the geostrophic basic state are theoretically unstable.

Vertical profiles of the critical temperature gradient were constructed for each case. The buoyancy frequency N^2 was calculated using the sounding nearest to the band. Figure 11a–e shows these profiles computed for moist and dry adiabatic ascent and descent, along with the observed cross-band temperature gradient estimated as described above.

In each case there are regions that are potentially unstable. In these regions the critical temperature gradient can be computed only for dry conditions. Note that regions of potential instability in a baroclinic atmosphere are also potentially symmetrically unstable. The region of symmetric instability as previously assessed from the single-sounding Richardson number analysis is indicated on each figure and is hereafter referred to as the RSI. For the case of 11 December 1982 which has no RSI, the LMI is indicated.

In two of the five cases, 5 December 1981 and 11 January 1984, the RSI corresponds to a region of near-neutral moist symmetric stability as assessed from the temperature gradient analysis (TGA). In both of these cases, the RSI corresponds to a region of the atmosphere that is at or near saturation and where the critical temperature gradient for moist adiabatic ascent is close to the observed temperature gradient.

On 20 December 1982, the atmosphere is not saturated in the RSI. While there is potential instability to upright convection in this region, the TGA indicates that the atmosphere is stable to dry symmetric overturning. However, above the RSI, there are numerous

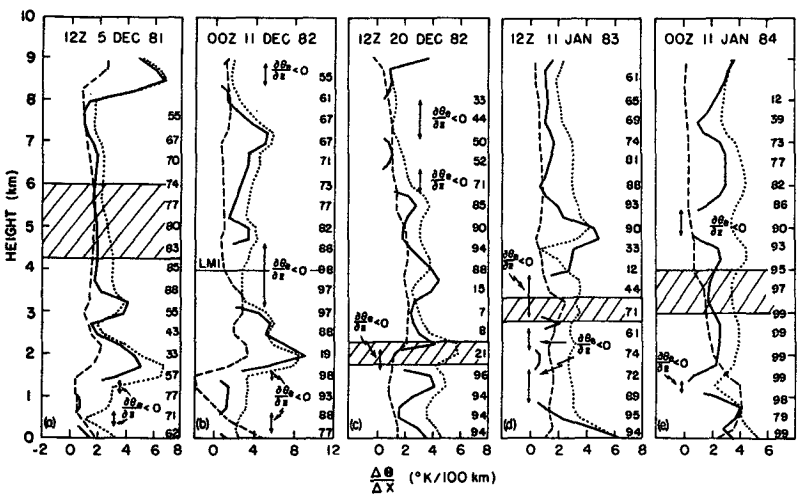

FIG. 11. Cross-band temperature gradient (K/100 km) as a function of height (km) for (a) 1200 GMT 5 December 1981, (b) 0000 GMT 11 December 1982, (c) 1200 GMT 20 December 1982, (d) 1200 GMT 11 January 1983, (e) 0000 GMT 11 January 1984. Observed temperature gradient (dashed), critical temperature gradient for dry symmetric instability (dotted), critical temperature gradient for moist symmetric instability (solid). Region of instability as assessed from Richardson number analysis is hatched. Relative humidity (%) is indicated on the right-hand side of each panel.

instances where the dry or moist instability criteria are either approached, met or exceeded.

On 11 January 1983 the situation is very similar. The RSI is unsaturated, potentially unstable to upright convection and stable to dry symmetric overturning. There is a region of the atmosphere above the RSI (near 6 km) where the atmosphere is saturated and the TGA shows slight moist symmetric instability. Finally, the case of 11 December 1982 which has no RSI shows a narrow region of dry symmetric instability at 3.25 km. In the vicinity of the LMI (from 3 to 4.5 km) the atmosphere is saturated and convectively unstable.

To properly assess the symmetric stability using the geostrophic wind shear, a good estimate of the observed temperature gradient is required. The measured temperature gradient used in the above analyses was made using only two soundings and probably represents an underestimate of the actual temperature gradient. Nonetheless, it is noteworthy that the estimated temperature gradient rarely exceeds the critical value.

4. Conclusions and discussion

This study was undertaken to examine the possible role of symmetric instability in the formation of precipitation bands. Observations from 15 cases of banded and nonbanded precipitation were used for this purpose. The observations agree with certain aspects of the present linear theory.

In nine of the 11 band cases, the band orientation is within 15 deg of both the 1000–500 mb geostrophic shear direction and the actual shear direction at the level of maximum instability. Shallow layers (0.5–2.0 km depth) of strong band-parallel shear in the middle troposphere, typically having magnitudes of 10–20 m s^{-1} km^{-1}, are observed to accompany the occurrence of banded precipitation. Substantial shears of 5–10 m s^{-1} km^{-1} over very deep layers in the atmosphere are also observed when bands occur. Observations provide evidence that the bands are quasi-two-dimensional with most of the horizontal variations in thermodynamic and kinematic properties occurring in the cross-band direction. Finally, the spacing between bands agrees with the predictions of the linear theory.

Single sounding analysis techniques from both the linear and parcel theories of symmetric instability showed that in the cases where bands were observed, regions of the atmosphere were symmetrically unstable. These results are consistent with the results of Bennetts and Sharp (1982) who showed that the theoretical growth rate of symmetric instability can be used as a good predictor of banded precipitation.

The analysis techniques used in this study depend on a knowledge of the vector geostrophic wind shear. In assessing the symmetric instability of the atmosphere for each case, the observed band-parallel wind shear as measured from a single sounding was assumed to represent the geostrophic basic state. In Section 3 we showed, based on a two-sounding estimate of the geostrophic wind shear, that this assumption may not be justified.

Stability analyses using the estimated geostrophic shear were performed and found to differ from those using the actual wind shear. If the actual wind shear is different from the estimated geostrophic shear, there are two possible reasons. One is that the flow is not in thermal wind balance. In this case the stability criterion for symmetric instability is yet to be determined and it would not be appropriate to use the conventional Richardson number criterion. The other possibility is that there are local variations in the temperature gradient. In this case, the two-sounding estimate of temperature gradient used to calculate the geostrophic shear may produce erroneous results. More accurate measurements of the geostrophic basic state will be required in future studies in order to address these issues.

We have pointed out that the present theory does not explain the apparent propagation of some bands relative to the observed cross-band flow, though this flow may be strongly influenced by the band circulations. In addition, the theory may have to be expanded to account for effects such as curved flow, non-unidirectional shear and perhaps nonlinear transports.

Linking symmetric instability with banded precipitation can have major consequences. Operationally, the prediction of when and where bands will form and in what direction they will move is vital to improving mesoscale forecasts. Furthermore, such an instability may have important effects on the large-scale flow. Stone (1972) and Emanuel (1983a) have both suggested that symmetric instability can result in appreciable transports of heat and momentum. If symmetric instability is responsible for the observed bands that occur so often in extratropical cyclones, the resulting heat and momentum transports should be more closely studied. A parameterization for such transports may be necessary in the current large-scale numerical models.

Acknowledgments. This work represents part of the first author's Master's thesis at M.I.T. The authors thank Prof. Peter Stone for his insightful comments. The first author thanks Stephen Garner for the many hours of discussion concerning the thesis. Special thanks go to Spiros Geotis and Pauline Austin for their review of this manuscript and to Isabelle Kole and Michael Rocha for drafting the figures.

REFERENCES

Bennetts, D. A., and B. S. Hoskins, 1979: Conditional symmetric instability—a possible explanation for frontal rainbands. *Quart. J. Roy. Meteor. Soc.*, **105**, 945–962.

——, and J. C. Sharp, 1982: The relevance of conditional symmetric instability to the prediction of mesoscale frontal rainbands. *Quart. J. Roy. Meteor. Soc.*, **108**, 595–602.

Durran, D. R., and J. B. Klemp, 1982: On the effects of moisture on the Brunt-Väisälä frequency. *J. Atmos. Sci.*, **36,** 2425–2449.

Eliassen, A., 1962: On the vertical circulation in frontal zones. *Geofys. Publ.*, Bjerknes Memorial Vol., 147–160.

Emanuel, K. A., 1979: Inertial instability and mesoscale convective systems. Part I. Linear theory of inertial instability. *J. Atmos. Sci.*, **36,** 2425–2449.

——, 1983a: The Lagrangian parcel dynamics of moist symmetric instability. *J. Atmos. Sci.*, **40,** 2368–2376.

——, 1983b: On assessing local conditional symmetric instability from atmospheric soundings. *Mon. Wea. Rev.*, **111,** 2016–2033.

Mann, H. B., and D. R. Whitney, 1947: On a test of whether one or two random variables is stochastically larger than the other. *Ann. Math. Statist.*, **18,** 50.

Ooyama, K., 1966: On the stability of baroclinic circular vortex: A sufficient criteria for instability. *J. Atmos. Sci.*, **23,** 43–53.

Parsons, D. B., and P. V. Hobbs, 1983: The mesoscale and microscale structure and organization of clouds and precipitation in mid-latitude cyclones. XI: Comparisons between observational and theoretical aspects of rainbands. *J. Atmos. Sci.*, **40,** 2377–2397.

Passarelli, R. E., N. D. Gordon and M. A. Seltzer, 1986: Case Study of an Intense Winter Snow Band: The Possible Role of Symmetric Instability. *J. Atmos. Sci.* (in press).

Solberg, H., 1936: Le mouvement d'inertie de l'atmosphere stable et son role dans la theorie des cyclones. Memoir presented to the Meteor. Assoc. of the U.G.G.I., Lisbon, Dupont Press.

Stone, P. H., 1966: On non-geostrophic baroclinic stability. *J. Atmos. Sci.*, **23,** 390–400.

——, 1972: On non-geostrophic baroclinic stability: Part III. The momentum and heat transports. *J. Atmos. Sci.*, **29,** 419–426.